2011

Direct simulation Monte Carlo study of effects of thermal nonuniformities in electron-beam physical vapor deposition

A Venkattraman
Purdue University

Alina A. Alexeenko
Purdue University - Main Campus, alexeenk@purdue.edu

Direct simulation Monte Carlo study of effects of thermal nonuniformities in electron-beam physical vapor deposition[a)]

A. Venkattraman
School of Aeronautics and Astronautics, Purdue University, West Lafayette, Indiana 47907

Alina A. Alexeenko[b)]
School of Aeronautics and Astronautics, Purdue University, West Lafayette, Indiana 47907 and Birck Nanotechnology Center, Purdue University, West Lafayette, Indiana 47907

(Received 8 December 2010; accepted 1 May 2011; published 10 June 2011)

In a typical electron-beam physical vapor deposition system, there is limited control over how the high-power electron beam heats the metal surface. This leads to thermal nonuniformities at the melt. Three-dimensional direct simulation Monte Carlo simulations were performed with the aim of quantifying the effect of such spatial variations of source temperature in thin film depositions using an electron-beam physical vapor deposition system. The source temperature distribution from a typical deposition process was used in the direct simulation Monte Carlo simulations performed for various mass flow rates. The use of an area-averaged temperature is insufficient for all mass flow rates due to the highly nonlinear relationship between temperature and saturation number density, and hence, the mass flux. The mass flow rate equivalent temperature was determined, and the simulations performed with this temperature were compared with those corresponding to the actual nonuniform temperature distribution. For low mass flow rates, the growth rates depend very weakly on the spatial variation of temperature as long as an equivalent temperature corresponding to the same mass flow rate was used. However, as the mass flow rate increases, the error associated with this approximation increases. For deposition processes with source Knudsen numbers less than 0.05, it is not possible to account for the spatial nonuniformities in temperature using the total mass flow rate without significant errors. For a given mass flow rate, the errors associated with using an equivalent temperature decrease with increasing collector plane distance since the flow is allowed to expand further, thereby decreasing the effects of slit temperature nonuniformities. © *2011 American Vacuum Society*. [DOI: 10.1116/1.3592890]

I. INTRODUCTION

Thin films find applications in various technologies ranging from nano- and microelectromechanical systems[1] to optics and coatings in aerospace systems. Thin films of conductors, insulators, and semiconductors used in the fabrication of microelectronic devices,[2] high-precision mirrors, and thermal barrier coatings used in gas turbine engines to improve performance and reliability are some examples of the applications of thin films. Among the various methods that can be used to deposit thin films including chemical vapor deposition,[3] molecular beam epitaxy,[4] sputtering of particles by energetic ion bombardment,[5] etc., the electron-beam physical vapor deposition (EBPVD) remains one of the most widely used techniques.[6] Some of the advantages[7] of EBPVD include its wide range of deposition rates from 0.01 to 100 μm/min, favorable low stress levels in the deposited films, well-controlled grain structure, and efficient energy utilization.[8]

The ability to simulate such deposition processes and predict the properties of thin films including the growth rate, nonuniformity, and grain structure gain further importance due to the cost involved in performing these deposition experiments. Modeling such processes can also be useful in the design of these vacuum deposition systems. In order to make accurate predictions using numerical simulations, it is imperative to ensure that the simulations mimic the real deposition processes as closely as possible. This requires some effort dedicated to not just developing models but also to assess the importance of various parameters that are inputs to these models.

All vacuum deposition processes mentioned earlier, including the EBPVD, produce supersonic jets that expand into vacuum and impinge on a substrate creating the solid film.[9] Such supersonic jets often involve significant thermal nonequilibrium. In order to predict the jet properties and the resultant thin film properties, a description of vapor flow based on nonequilibrium kinetic theory of gases is required. The direct simulation Monte Carlo (DSMC) method[10] is the most powerful and popular numerical approach for solution of gas kinetic problems for supersonic flows. Also, it can be used to simulate vapor flows expanding into vacuum from sources of complex geometries frequently encountered in deposition systems.[11] Accurate modeling of vapor flows using the DSMC method can help in predicting the intricate details of the thin films that are deposited using these vacuum processes. The fidelity of such DSMC simulations is, however, strongly dependent on the accuracy of input parameters such as molecular interaction models, gas-surface interaction, and parameters used in the boundary conditions.

[a)]This article is based on material presented at the 57th International Symposium of the American Vacuum Society.
[b)]Electronic mail: alexeenk@purdue.edu

In our previous work,[12] we considered various molecular models and by comparison of mass fluxes at the substrate location obtained using the DSMC simulations with those measured in experiments, a molecular model for copper vapor was determined. However, in order to be able to best represent experimental conditions in the DSMC simulations, other parameters such as temperature distribution in the source are likely to be equally important because the source temperatures determine the mass flow rate, which in turn affects the film properties in a number of ways. For instance, in EBPVD, it is not possible for the electron beam to uniformly heat the metal surface. The main goal of this work is to quantify the effects of source temperature nonuniformity in the DSMC simulations performed to model thin films deposited using the EBPVD technique. In particular, we address the question of how to best account for such spatial variations of temperature in the source.

The remainder of the paper is organized as follows. Section II provides the background information on EBPVD and the need to quantify the effects of spatial variations of the source temperature. Section III describes the numerical simulation approach including the flow conditions and details of the computational domain and the DSMC simulation parameters used. Section IV presents the results and discusses the same with Sec. V reserved for conclusions.

II. EBPVD: OVERVIEW OF THE TECHNIQUE AND PROCESS VARIABLES

The EBPVD technique uses an energetic electron beam to initially melt and then vaporize the metal of interest after which the metal vapors are expanded into vacuum to be deposited on a substrate at some distance from the source. The electron beam is focused on a certain region and while part of the energy of the beam is used to heat the metal,the remainder is used to provide the heat of vaporization to convert the molten metal to the vapor state. Though the electron beam is concentrated in a certain region, the conduction through the metal results in the beam heating up the surrounding regions as well. As a result, there is limited control over how the energetic electron beam heats the metal and leads to temperature gradients at the melt surface. Even if the temperatures of the surrounding regions are not as high, they do contribute to the total mass flow rate of the metal vapor from the slit, thereby contributing to the mass flux at the substrate.

Figure 4(b) of the paper by Thakur and Sahu[13] shows a digital photograph taken during their experiments, clearly showing the spatial variation of the thermal radiation intensity and, hence, the slit temperature. In order to characterize quantitatively the importance of specifying an accurate source temperature distribution in the DSMC simulations, we use representative intensity distributions from their work and convert them into temperatures. Though the intensity and, hence, temperature might vary from one experiment to another and, potentially, from one mass flow rate to another, it suffices to use one such realistic distribution to ascertain the effect of spatial variation of temperature on mass flux at the substrate location. Hence, the normalized temperature variation was obtained from the intensities reported by Thakur and Sahu,[13] while the actual magnitudes of temperature used in the DSMC simulations were scaled in order to obtain various mass flow rates. The intensity of thermal radiation was related to temperature as

$$I \propto T^4, \tag{1}$$

which assumes that the background temperature is much lower than that of the source.

In earlier works,[13,14] which used a cosine power law to fit the experimental data, the nonuniformity in source temperature was typically accounted for by using an area-averaged temperature. However, it should be mentioned that the mass flow rate obtained using the area-averaged temperature would not be the same as the area-averaged mass flow rate due to the highly nonlinear relationship between temperature and corresponding mass flux. The results presented in this work show significant differences in mass fluxes at the substrate location obtained using an area-averaged temperature and the actual nonuniform slit temperature distribution.

III. DSMC SIMULATION PARAMETERS AND FLOW CONDITIONS

The DSMC simulations performed in this work closely mimic the experimental set-up used by Sahu and Thakur[13,14] in earlier studies of electron-beam deposition of copper from a slit source. Only the key aspects of the set-up are presented here. The experimental set-up with details of the electron gun can be found in Refs. 13 and 14. Figure 1 shows a schematic of the deposition set-up and the computational domain used in our simulations. The temperature distribution along the length of the slit is not exactly symmetric about the center of the slit and, hence, the flow field is not symmetric about $Y = 0$ plane. However, symmetry about $Z = 0$ has been exploited in our simulations. The computational domain extends from $Z = 0.0$ to $Z = 0.164$ m in the Z-direction and from $Y = -0.164$ to $Y = 0.164$ m in the Y-direction. The collector plane is at a distance of 0.14 m

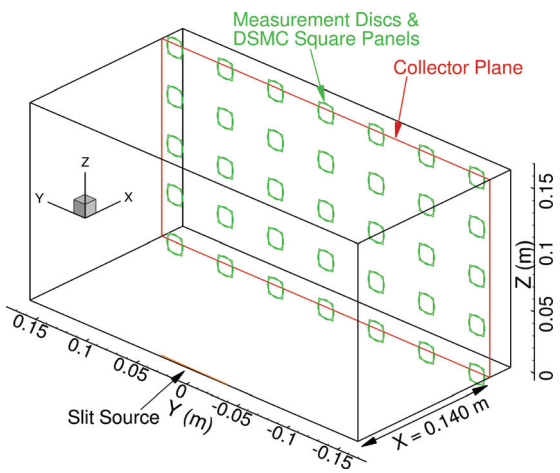

FIG. 1. (Color online) Schematic of experimental set-up and the computational domain used in the DSMC simulations.

TABLE 1. Summary of the DSMC simulations.

Case I: Medium mass flow rate		
(a) Nonuniform slit temperature	(b) Uniform slit temperature with the same mass flow rate as case I (a)	(c) Uniform slit temperature same as T_{avg} for case I (a)
$T_{min} = 1574\ 8$ K $T_{max} = 1828.1$ K $T_{avg} = 1728.9$ K $\dot{m} = 82.8$ mg/s Kn = 0.0293	$T = 1744.3$ K $\dot{m} = 82.8$ mg/s Kn = 0.0739	$T = 1728.9$ K $\dot{m} = 68.5$ mg/s Kn = 0.0884
Case II: Low mass flow rate		
(a) Nonuniform slit temperature	(b) Uniform slit temperature with the same mass flow rate as case II(a)	
$T_{min} = 1443.6$ K $T_{max} = 1675.8$ K $T_{avg} = 1584.8$ K $\dot{m} = 12.4$ mg/s Kn = 0.1687	$T = 1600.2$ K $\dot{m} = 12.4$ mg/s Kn = 0.4569	
Case III: High mass flow rate		
(a) Nonuniform slit temperature	(b) Uniform slit temperature with the same mass flow rate as case III(a)	
$T_{min} = 1749.8$ K $T_{max} = 2031.3$ K $T_{avg} = 1921.0$ K $\dot{m} = 669$ mg/s Kn = 0.0043	$T = 1936.4$ K $\dot{m} = 669$ mg/s Kn = 0.0101	

from the slit source, which is the same as the distance in the experimental setup.[13]

The DSMC simulations give the average mass flux at a specific surface element based on the number of molecules striking it. In order to ensure that the simulations represent the experimental set-up as accurately as possible, the area of the square elements on which the mass fluxes are computed was taken to be the same as the area of the circular disks that have been used to measure the mass of copper deposited on them. The diameter of these circular measurement disks is given[14] as 16 mm corresponding to an area of 2.01 cm^2 and, hence, the side of the square panels used in the DSMC simulations is about 14 mm. The slit temperature distribution that was obtained using intensities from Thakur and Sahu[13] as described earlier was used along with the corresponding saturation number density (n). The variation of saturation vapor pressure (P) with temperature is given by

$$P = \exp\left[-\frac{\Delta H}{R_u}\left(\frac{1}{T} - \frac{1}{T_{P=1}}\right)\right], \tag{2}$$

where ΔH is the enthalpy of vaporization, R_u is the universal gas constant, P is the vapor pressure in Pa, T is the temperature at which the vapor pressure is required in units of K, and $T_{P=1}$ is the temperature at which the vapor pressure is 1 Pa. For copper, which is the metal used in our simulations, the parameters[15] used were $\Delta H = 313.2$ kJ/mol and $T_{P=1} = 1511.8$ K. Once the saturation vapor pressure is computed, the saturation number density is obtained using the ideal gas law

$$P = nkT, \tag{3}$$

where k is the Boltzmann's constant. The mass flux from a given location in the source is given by[10]

$$m_f = \frac{1}{4}Mn\bar{c}, \tag{4}$$

where M is the atomic mass of copper (1.055×10^{-25} kg), n is the saturation number density corresponding to the saturation vapor pressure given by Eq. (2), and $\bar{c}$ is the average velocity given by[10]

$$\bar{c} = \sqrt{\frac{8kT}{\pi M}}. \tag{5}$$

Hence, the mass flux at a given location in the source depends only on the local temperature (T) because both n and $\bar{c}$ are determined using T. The total mass flow rate from the slit ($\dot{m}$) is calculated by integrating the mass fluxes obtained using Eq. (4) over the slit area. Hence, for a nonuniform slit temperature profile, the mass flow rate is obtained as

$$\dot{m} = \frac{1}{4}M\int_{A_{slit}} n\bar{c}dA, \tag{6}$$

where A_{slit} is the slit area. In this work, since the temperature is extracted only in discrete points, the integration was performed numerically. For a slit with uniform slit temperature and, hence, uniform mass flux from all locations of the slit, no integration is required, and the total mass flow rate from the slit is given by

$$\dot{m} = \frac{1}{4}Mn\bar{c}A_{slit}. \tag{7}$$

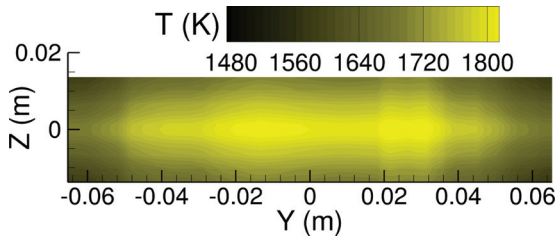

FIG. 2. (Color online) Slit temperature contours for case I(a).

It should be mentioned that Eq. (4) is the equilibrium flux for a stationary gas. In this work, the metal vapor is considered to have a zero average velocity when it effuses from the slit. In case an application with nonzero average velocity has to be simulated, the corresponding expression for equilibrium flux (see, for example, Eq. (4.22) of Bird[10])

While performing the DSMC simulations, the only flow condition related input that is given to the DSMC solver is the temperature distribution, which is then used to compute the saturation number density distribution and, hence, the mass flux distribution. All DSMC simulations presented in this work were performed using the 3D version of the SMILE (Ref. 16) software system. The DSMC simulation parameters used in the simulation are summarized below. The ratio of real to simulated molecules was varied between 1×10^9 and 5×10^{10} depending on the flow conditions and was chosen in such a way that there were at least 100 particles per cubic mean free path (λ^3). The expression for mean free path (λ) at a given number density and temperature for a variable hard sphere (VHS) model is given by[10]

$$\lambda = \frac{1}{\sqrt{2}\pi d_{\mathrm{ref}}^2 n (T_{\mathrm{ref}}/T)^{\omega-1/2}}, \tag{8}$$

where d_{ref}, T_{ref}, and ω are parameters of the VHS model. We used a VHS model whose parameters[12] can be summarized as $d_{\mathrm{ref}} = 0.45$ nm at $T_{\mathrm{ref}} = 300$ K and $\omega = 0.92$. The time step was varied from 1×10^{-7} to 1×10^{-6} s and was chosen in such a way that it was less than the estimated mean

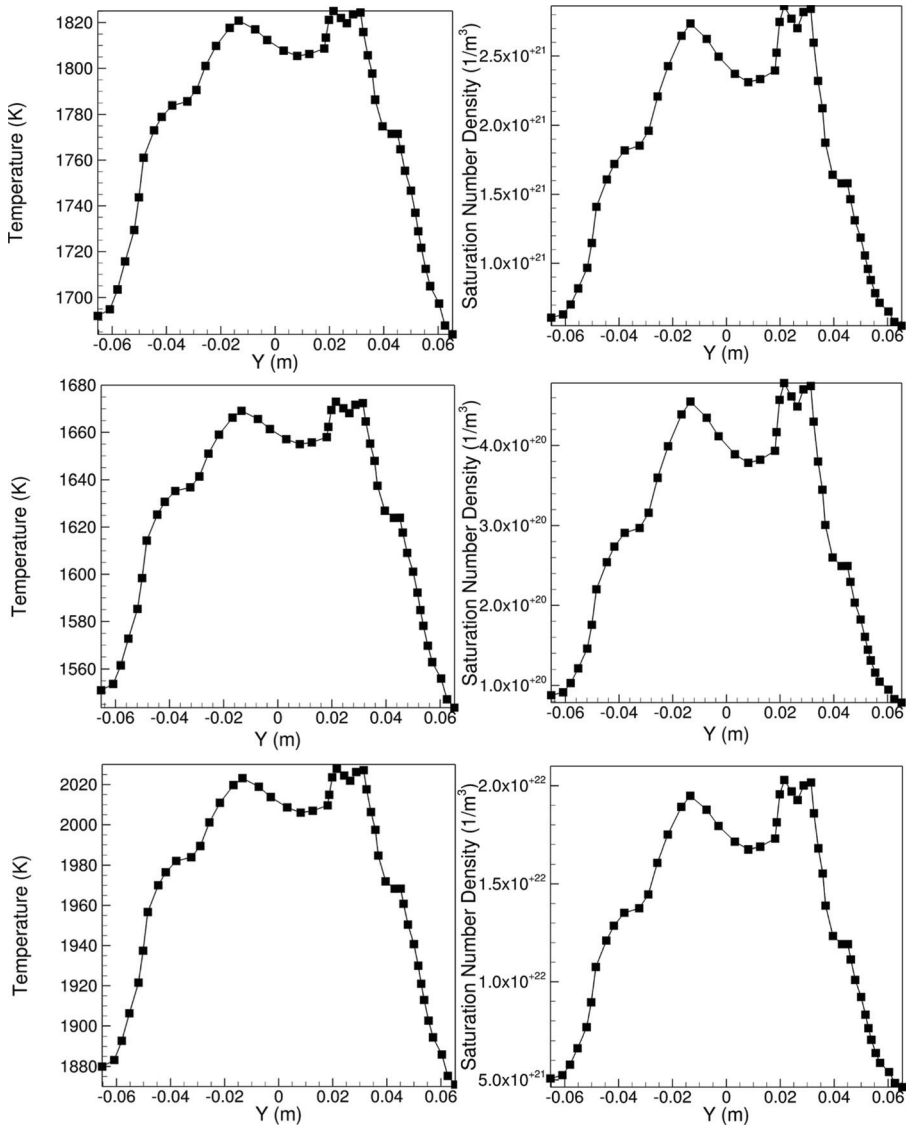

FIG. 3. Slit temperature and saturation number density distribution at $Z = 0$ for cases I(a), II(a), and III(a).

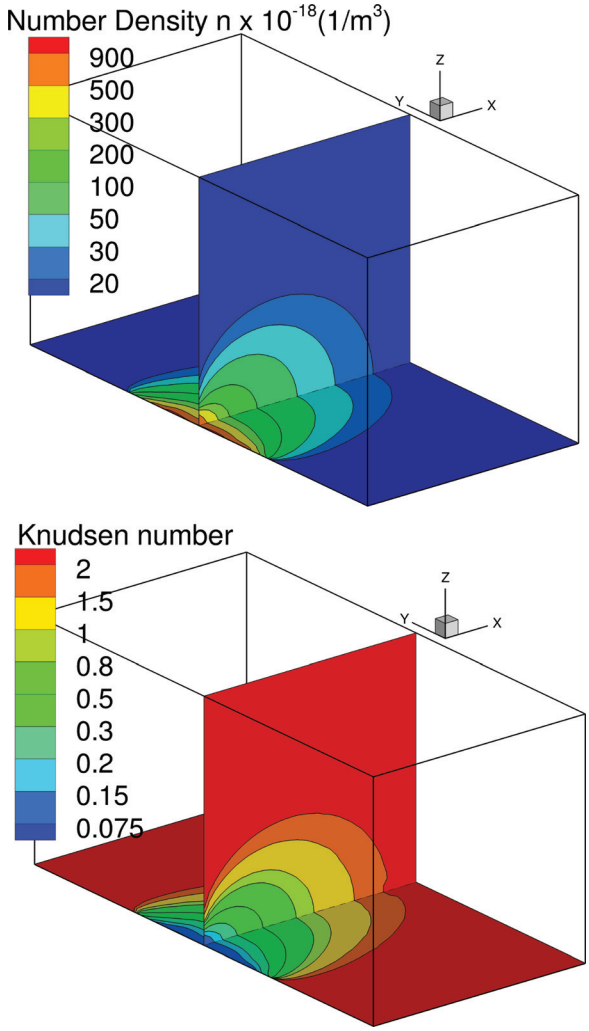

FIG. 4. (Color online) Number density and Knudsen number contours for case I(a).

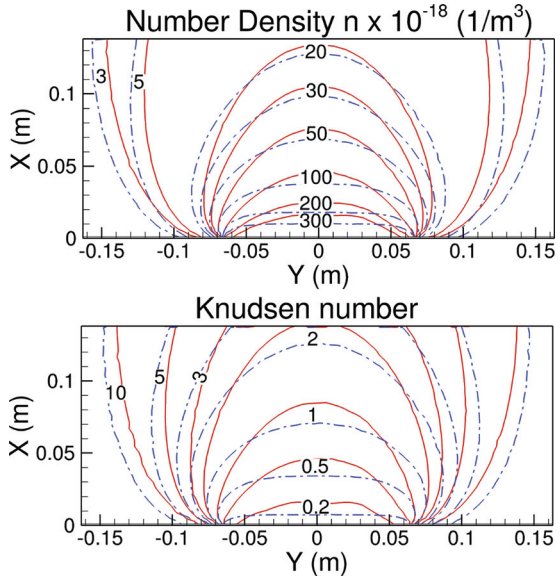

FIG. 5. (Color online) Comparison of number density and Knudsen number contours at the $Z = 0$ plane for cases I(a) (———) and I(b) (– – –).

residence time of a molecule in a collision cell and also less than the mean collision time. The collision cell size was ensured to be smaller than the mean free path to ensure good spatial resolution. The slit source was simulated as an inflow boundary with molecules introduced into the computational domain using the given spatial temperature distribution and the corresponding saturation number density distribution. While cases I(a), II(a), and III(a) have a nonuniform distribution of temperature and, hence, saturation number density, cases I(b), I(c), II(b), and III(b) have uniform temperatures. The details of the simulation conditions for each case are summarized in Table 1.

IV. RESULTS AND DISCUSSION

The 3D DSMC simulations of metal vapor flow from the electron-beam source set-up shown in Fig. 1 were performed for various mass flow rates from the slit source. In this work, we consider three different mass flow rates as mentioned before. For each mass flow rate, both uniform and

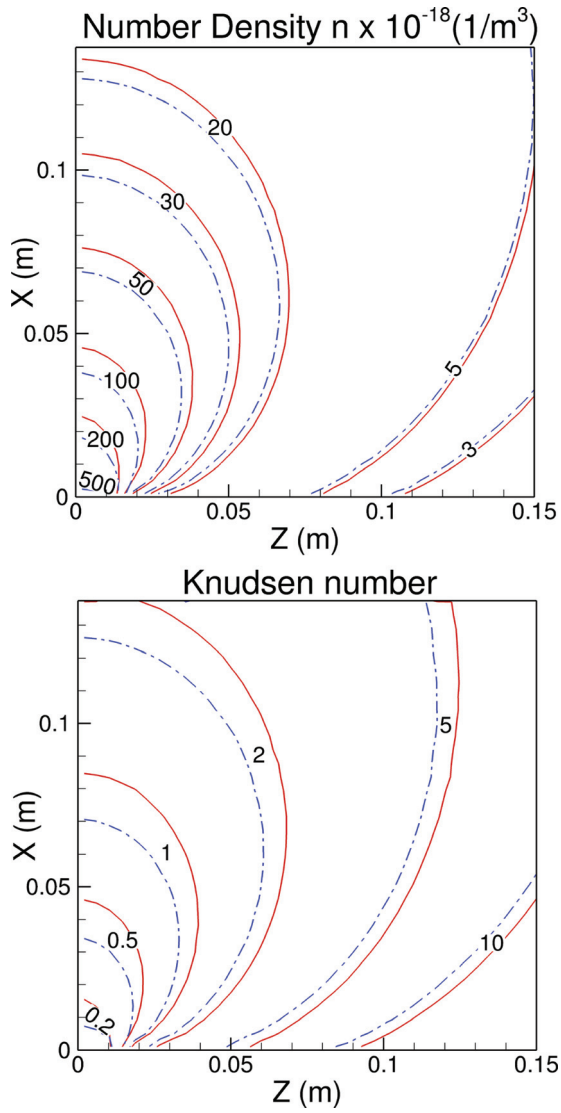

FIG. 6. (Color online) Comparison of number density and Knudsen number contours at the $Y = 0$ plane for cases I(a) (———) and I(b) (– – –).

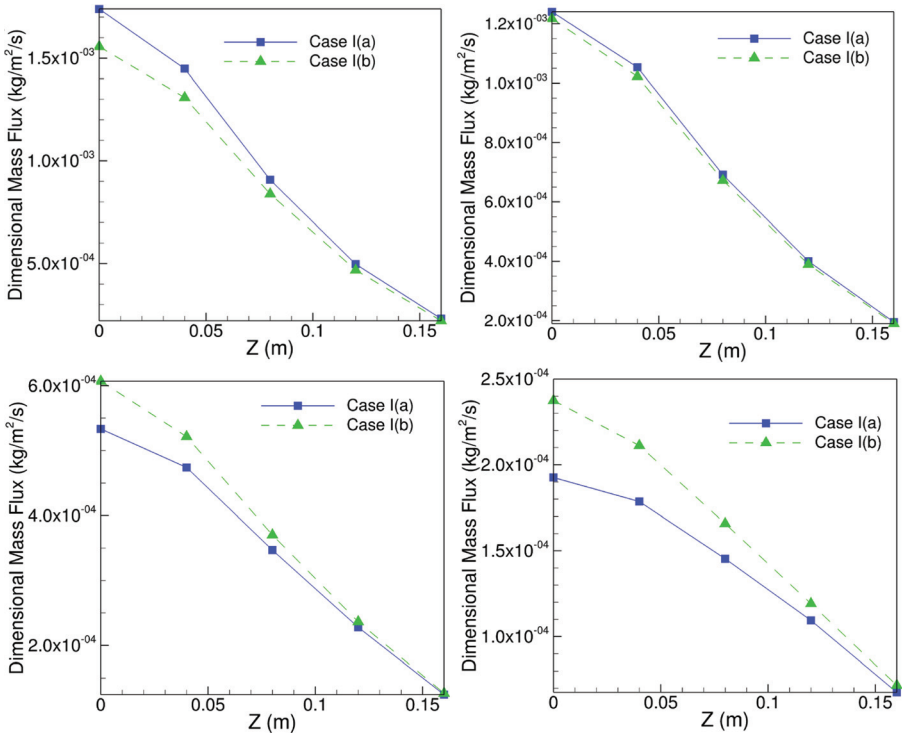

FIG. 7. (Color online) Comparison of mass flux at all collector plate locations for cases I(a) and I(b) for a collector plane distance of $X = 0.14$ m. (Top-left) $Y = 0.0$; (top-right)$Y = 0.05$; (bottom-left)$Y = 0.10$; (bottom-right)$Y = 0.15$ m.

nonuniform slit temperature distributions are considered. As described earlier, the temperature variations for the latter were taken from deposition experiments.[13] The length and width of the slit were chosen as 130.6 mm × 27.4 mm. Though intensity data are available[13] for a larger slit length, the low temperatures in these regions ensure that their contribution to the mass flow rate is negligible.

The details of all DSMC simulations performed in this work are summarized in Table 1 and are described in detail below. Case I(a) has a nonuniform slit temperature distribution (and hence mass flux distribution) with a maximum temperature of 1828.1 K and a minimum temperature of 1574.8 K, such that the total mass flow rate through the slit is 82.8 mg/s. Figure 2 shows the slit temperature contours for case I(a) with the contours plotted in a two color format to enable qualitative comparison with the digital photograph of experiments by Thakur and Sahu [13] shown in Fig. 4(b).[13] Figures 3(a) and 3(b) show the temperature and saturation number density variation as a function of Y in the $Z = 0$ plane.

Case I(b) is a case with uniform slit temperature, which was calculated in such a way that the mass flow rate obtained was the same as case I(a), which was 82.8 mg/s. It should be mentioned that even though the mass flow rates have been matched for cases I(a) and I(b), the energies of the atoms leaving the slit will be different due to the different temperatures. This is not an issue for the purpose of this work since we concentrate on computing the growth rates at the substrate location as opposed to the actual grain structure details, which would depend on the energies of the atoms reaching the substrate. However, to compute the grain structure and growth rates accurately an equivalent uniform temperature will not be sufficient. Case I(c) is a case with uniform slit temperature, which was equal to the area-averaged temperature of case I(a). Using the area-averaged slit temperature results in a mass flow rate of 68.5 mg/s, which is about 20% less than case I(a).

Case II(a) has a nonuniform slit temperature distribution (and hence mass flux distribution), which is a scaled down version of case I(a). The lower temperatures result in a lower mass flow rate from the slit when compared to case I(a). The maximum and minimum temperatures for this case are 1675.8 and 1443.6 K, respectively. Case II(b) corresponds to a case with uniform slit temperature, which was calculated in such a way that the mass flow rate obtained was the same as case II(a) and equal to 12.4 mg/s. Case III(a) has a nonuniform slit temperature distribution (and hence mass flux distribution), which is a scaled up version of case I(a). The higher temperatures result in a higher mass flow rate from the slit when compared to case I(a). The maximum and minimum temperatures for this case are 2031.3 and 1749.8 K, respectively. Case III(b) corresponds to a case with uniform slit temperature, which was calculated in such a way that the mass flow rate obtained was the same as case III(a) and is equal to 669 mg/s. Figure 3 also shows the temperature and saturation number density variation as a function of Y in the $Z = 0$ plane for cases II(a) (low mass flow rate, nonuniform case) and III(a) (high mass flow rate, nonuniform case).

The Knudsen numbers listed for each of the cases in Table 1 were defined as the ratio of mean free path (λ) to the characteristic length, which in this case is the slit width and we get

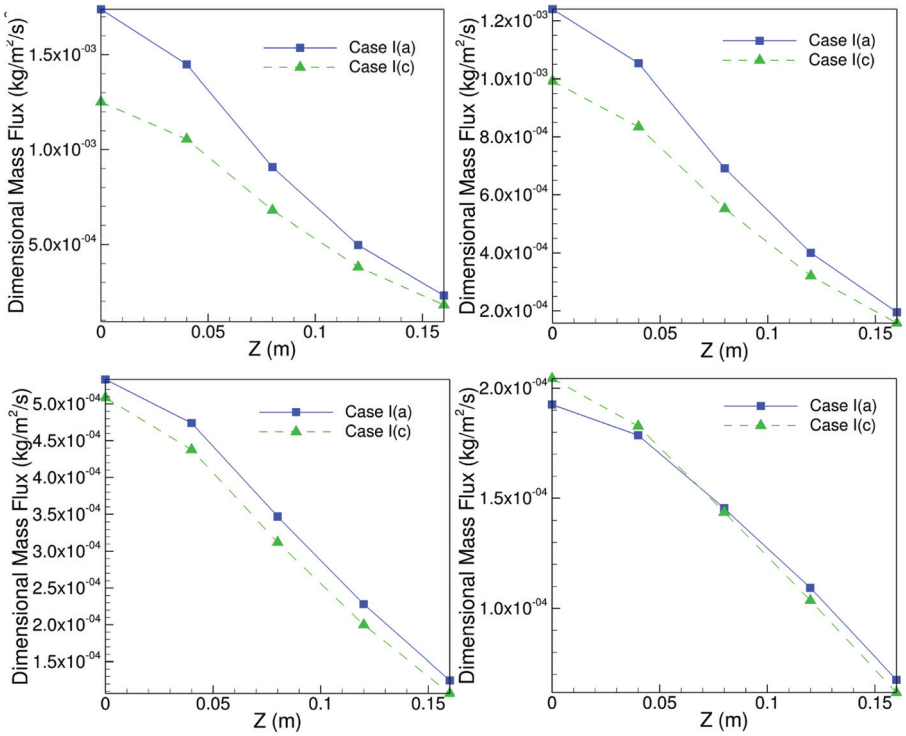

FIG. 8. (Color online) Comparison of mass flux at all collector plate locations for cases I(a) and I(c) for a collector plane distance of $X = 0.14$ m. (Top-left) $Y = 0.0$; (top-right)$Y = 0.05$; (bottom-left)$Y = 0.10$; (bottom-right)$Y = 0.15$ m.

$$\mathrm{Kn} = \frac{\lambda}{W}, \tag{9}$$

where W is the slit width equal to 27.4 mm in our case. For cases with nonuniform temperature distribution (cases I(a), II(a), and III(a)), the maximum temperature was used to compute the mean free path and, hence, to define the Kn.

Typical three-dimensional (3D) DSMC flow fields are shown in Fig. 4 with contours of number density and the Knudsen number shown for case I(a). In order to increase the clarity of information, the number density contours are shown only in two slices corresponding to $Y = 0$ and $Z = 0$ planes in the 3D flow field. The flow that is rapidly expanding into vacuum is characterized by strong density gradients. The transition regime with Kn in the range of 0.1–1, where collisions cannot be neglected, can clearly be seen. Figures 5 and 6 compare the contours of number density and the Knudsen number for cases I(a) and I(b) in the $Z = 0$ and $Y = 0$ planes, respectively. Figure 7 compares the mass fluxes obtained at various locations at the collector plane for cases I(a) (nonuniform temperature) and I(b) (uniform equivalent temperature). The mass fluxes reported are based on square collector plates of area 2.01 cm^2. It should be mentioned that even though the slit temperature distribution was not symmetrical about the $Y = 0$ plane, the mass fluxes for a given value of Y differed by less than 1% from the mass flux of the collector plate at -Y. This is consistent with the findings of the experiments by Thakur and Sahu.[13] Therefore, the mass fluxes reported for a given value of Y were obtained as the average of mass fluxes of collector plates at Y and -Y. The mass flux on collector plates at $Y = 0$ m and $Y = 0.05$ m is higher for case I(a) than case I(b), while the mass flux on collector plates at $Y = 0.10$ m and $Y = 0.15$ m is higher for case I(b) than case I(a). This trend can be explained using the number density contours obtained for the two cases. The number density contours clearly show that case I(a) has number densities higher than case I(b) in regions closer to the center of the slit and has number densities lower than case I(b) in regions away from the center of the slit. Hence, the actual vapor flow from the slit has a preference to collector plates located close to the center of the slit, while the uniform source corresponding to the same mass flow rate does

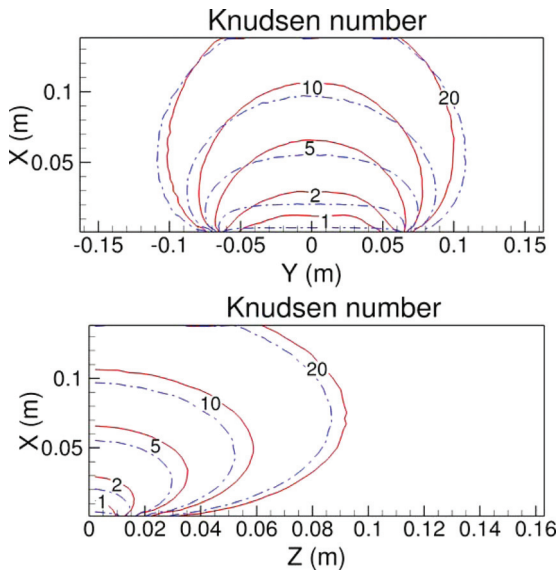

FIG. 9. (Color online) Comparison of contours of Knudsen number contours for cases II(a) (————-) and II(b) (– – –) in the $Z = 0$ and $Y = 0$ planes.

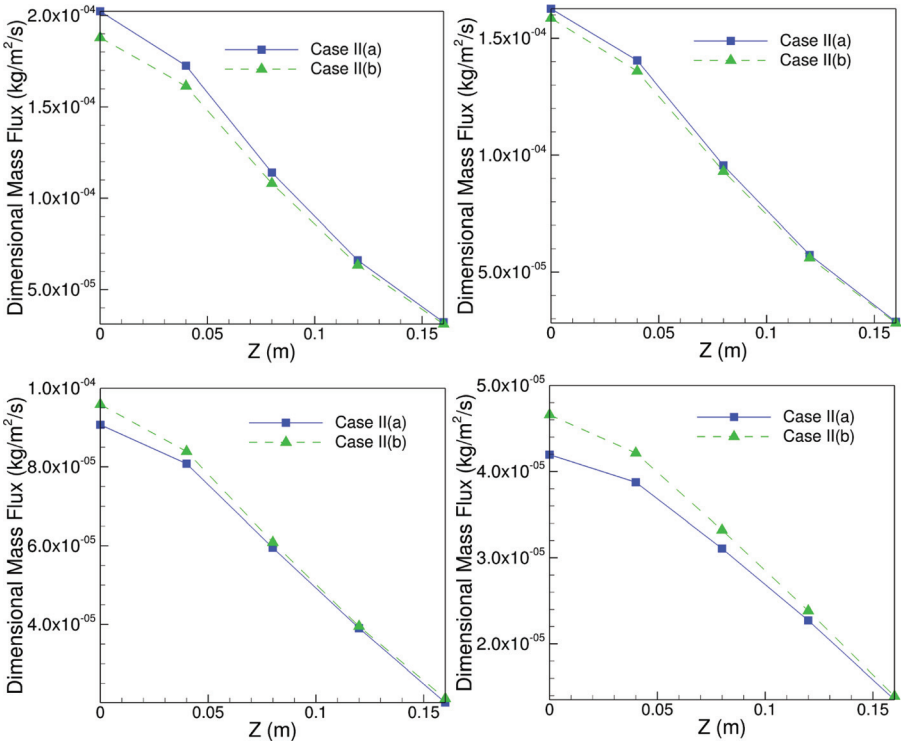

FIG. 10. (Color online) Comparison of mass flux at all collector plate locations for cases II(a) and II(b) for a collector plane distance of $X = 0.14$ m. (Top-left)$Y = 0.0$; (top-right)$Y = 0.05$; (bottom-left)$Y = 0.10$; (bottom-right)$Y = 0.15$ m.

not reproduce this characteristic, leading to differences in the collector plate mass fluxes. The maximum percentage difference in collector plate mass flux for the two cases is about 23% at the collector plate at $Y = 0.15$ m and $Z = 0$ m. The average error for all collector plates is a reasonable 7.9%. The fact that case I(b) has higher collector plate mass flux at some points and lower collector plate mass flux at the other points, when compared to case I(a), shows that the

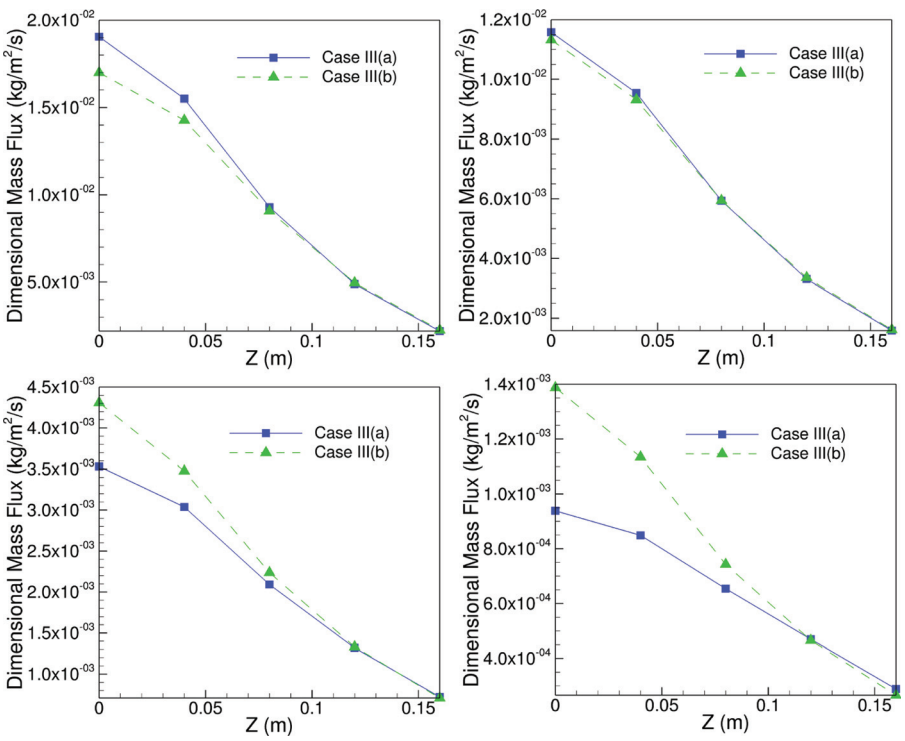

FIG. 11. (Color online) Comparison of mass flux at all collector plate locations for cases III(a) and III(b) for a collector plane distance of $X = 0.14$ m. (Top-left)$Y = 0.0$; (top-right)$Y = 0.05$; (bottom-left)$Y = 0.10$; (bottom-right)$Y = 0.15$ m.

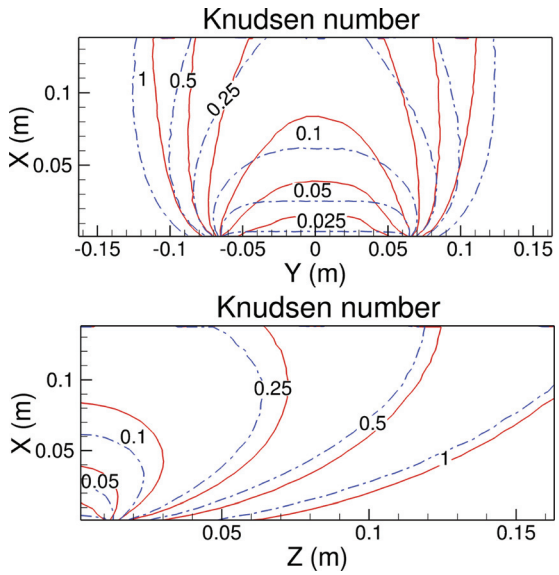

FIG. 12. (Color online) Comparison of contours of Knudsen number contours for cases III(a) (————) and III(b) (– – –) in the $Z = 0$ and $Y = 0$ planes.

normalized collector plate mass flux distribution (normalized using the respective maximum collector plate mass flux for each case) is different for the two cases. This is a direct consequence of the Knudsen number being different for the two cases.

Figure 8 compares the dimensional mass flux obtained using the actual nonuniform temperature profile [case I(a)] with that obtained using an area-averaged temperature [case I(c)]. It can be clearly seen that the area-averaged temperature profile underpredicts the mass fluxes at most of the collector plates (except a few collector plates farthest from the center of the slit). The differences are largely due to the nonlinear variation of mass flow rate with temperature, as a result of which an area-averaged temperature would not correspond to an area-averaged mass flow rate.

We then consider cases II(a) and II(b) that correspond to a lower mass flow rate of about 12.4 mg/s and, hence, would be closer to free-molecular flow. Similar to the previous case, Fig. 9 compares contours of the Knudsen number in the $Y = 0$ and $Z = 0$ planes for cases II(a) and II(b). Figure 10 compares the mass fluxes obtained for cases II(a) and II(b), and although the trend is somewhat similar, the differences are smaller than those obtained for the medium mass flow rate considered earlier. The maximum percentage difference in the collector plate mass flux is about 11% and occurs at the same collector plate at $Y = 0.15$ m and $Z = 0.0$. The average difference is also smaller when compared to the medium mass flow rate case at 4.6%.

Finally, the results are presented for cases III(a) and III(b) that correspond to the highest mass flow rate among the cases considered in this work. Figure 11 shows a comparison of the mass fluxes obtained for cases III(a) and III(b), and it can be seen that the differences are much larger than both the mass flow rates considered earlier. The maximum percentage difference in the collector plate mass flux is 47.9% and the average difference is 9.2%. Figure 12 compares contours of the Knudsen number for cases III(a) and III(b), and the flow is far from being completely expanded when it reaches the collector plane, thereby leading to much larger

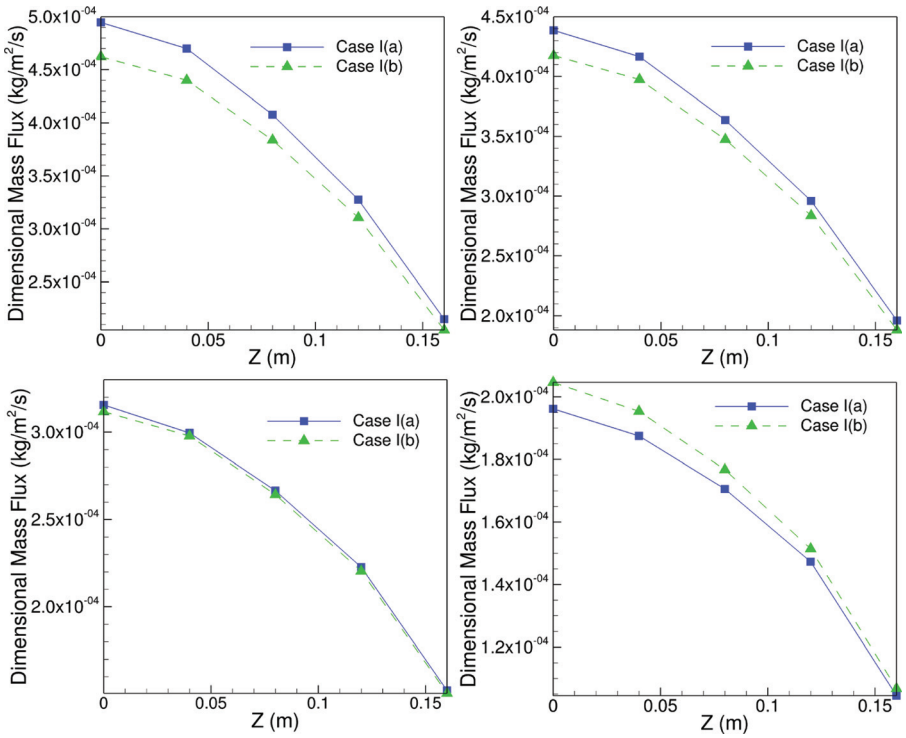

FIG. 13. (Color online) Comparison of mass flux at all collector plate locations for cases I(a) and I(b) for a collector plane distance of $X = 0.28$ m. (Top-left) $Y = 0.0$; (top-right) $Y = 0.05$; (bottom-left) $Y = 0.10$; (bottom-right) $Y = 0.15$ m.

errors in the collector plate mass fluxes than the cases considered earlier.

Based on the results obtained for the three mass flow rates, it is clear that using a constant slit temperature that corresponds to the same mass flow rate as the actual nonuniform slit temperature (and hence slit mass flux) leads to some errors in the collector plate mass flux. Though the magnitude of these errors was reasonable for the low mass flow rate case, it increased rapidly with increasing mass flow rate or decreasing Knudsen number. However, the results obtained are specific to the particular collector plane distance of $X = 0.14$ m from the slit source. In order to study the influence of changing the collector plane distance, simulations corresponding to case I(a) and case I(b) were repeated with the collector plane distance from the slit source doubled to $X = 0.28$ m. Figure 13 compares the collector plate mass fluxes for cases I(a) and I(b) with the increased collector plane distance of $X = 0.28$ m. As can be easily observed, the errors are significantly smaller than when the collector plane was at $X = 0.14$ m. The maximum and average errors are 6.6% and 3.6%, respectively. A similar trend was observed for cases III(a) and III(b) with the maximum and average errors decreasing to 7.7% and 3.54%, respectively, for the increased collector plane distance of $X = 0.28$ m. The reduction in error is due to the fact that the flow here is allowed to expand further before it reaches the collector plane, thereby decreasing the influence of slit temperature nonuniformities on the final collector plate mass flux.

V. CONCLUSIONS

The three-dimensional DSMC simulations were performed with the aim of quantifying the effect of spatial variation of slit temperature in thin film depositions using EBPVD. The slit temperature profile from a typical EBPVD process was used in the DSMC simulations performed for three different mass flow rates. The use of an area-averaged temperature was shown to underpredict the mass fluxes in all collector plates and, hence, insufficient to accurately simulate these deposition processes. This is largely due to the highly nonlinear relationship between the temperature and saturation number density and, hence, the mass flux. Simulations performed using a uniform slit temperature were shown to lead to better results as long as the equivalent slit temperature corresponding to the actual mass flow rate was used. However, both maximum and average errors associated with the equivalent temperature approximation were shown to increase as the mass flow rate was increased. For a collector plane distance of 0.14 m, the maximum error increased from about 10% for a mass flow rate of 12.4 mg/s ($\mathrm{Kn} \sim 0.4$) to about 47% for a mass flow rate of 669 mg/s ($\mathrm{Kn} \sim 0.01$). The reason for the trend was attributed to the fact that with an increase in mass flow rate (or decrease in the Knudsen number), the flow does not have a chance to completely expand by the time it reaches the collector plane. This was confirmed with the fact that for a given mass flow rate, the errors between the actual profile and the equivalent uniform temperature decreased as the collector plane was moved farther from the slit source, thereby allowing the flow to completely expand by the time it reaches the collector plates. This complete expansion ensures that slit nonuniformity effects become less important in predicting the mass flux and, hence, growth rates at the collector plane. Therefore, while it is shown that having the mass flow rate information of a deposition process will be sufficient to make reasonably accurate predictions of the growth rates at the substrate location, further research is required to improve the predictive capabilities of thin film deposition processes by coming up with nondimensional quantities that characterize the substrate distance required for a given flow to completely expand.

ACKNOWLEDGMENT

The authors would like to acknowledge the support from Kirk Endowment Seed Grant program, Birck Nanotechnology Center at Purdue University.

[1]J. J. Allen, *Micro-Electro Mechanical System Design* (CRC, Florida, 2005).
[2]M. Teng, X. He, and Y. Sun, Int. J. Mod. Phys. B **23**, 1910 (2009).
[3]J. H. Park and T. S. Sudarshan, *Chemical Vapor Deposition* (ASM International, Ohio, 2001).
[4]R. F. C. Farrow, *Molecular Beam Epitaxy: Applications to Key Materials* (Noyes, New Jersey, 1995).
[5]T. Itoh, *Ion Beam Assisted Film Growth* (Elsevier, Amsterdam, 1989).
[6]R. Bakish, *Introduction to Electron Beam Technology* (Wiley, New York, 1962).
[7]J. Singh and D. Wolfe, J Mater. Sci. **40**, 1 (2005).
[8]R. Stuart, *Vacuum Technology, Thin Films, and Sputtering: An Introduction* (Academic, New York, 1983).
[9]A. K. Rebrov, J. Vac. Sci. Technol. A **19**, 1679 (2001).
[10]G. A. Bird, *Molecular Gas Dynamics and the Direct Simulation of Gas Flows* (Oxford University, New York, 1994).
[11]K. Mukati, B. Ogunnaike, E. Eser, S. Fields, and R. Birkmire, Ind. Eng. Chem. Res. **48**, 5992 (2009).
[12]A. Venkattraman and A. A. Alexeenko, J. Vac. Sci. Technol. A **28**, 916 (2010).
[13]K. B. Thakur and G. K. Sahu, J. Phys. D **35**, 1812 (2002).
[14]G. K. Sahu and K. B. Thakur, Vacuum **81**, 77 (2006).
[15]J. Davis, *Copper and Copper Alloys* (ASM International, Ohio, 2001).
[16]M. S. Ivanov, A. V. Kashkovsky, S. F. Gimelshein, G. N. Markelov, A. A. Alexeenko, Ye. A. Bondar, G. A. Zhukova, S. B. Nikiforov, and P. V. Vaschenkov, "SMILE system for 2D/3D DSMC computations," in *25th International Symposium on Rarefied Gas Dynamics* (St. Petersburg Russia, 2006), pp. 21–28.